DOI:10.34918/85115

Michał BERNYŚ[1], Bartłomiej MELKA[1,*], Maria GRACKA[1], Ziemowit OSTROWSKI[1], Marek ROJCZYK[1], Krzysztof PSIUK-MAKSYMOWICZ[2], Damian BORYS[2], Jarosław WASILEWSKI[3], Jan GŁOWACKI[3], Ryszard BIAŁECKI[1]

Chapter 15. NUMERICAL MODELING OF BLOOD FLOW IN BIFURCATION AND TRIFURCATION GEOMETRIES USE OF DIFFERENT BOUNDARY CONDITIONS

15.1. Introduction

The study on 50 million people showed that the world's leading cause of death is ischemic heart disease, which is responsible for 11.3% of deaths, followed by a stroke with an 11% mortality rate [1]. Over the past 19 years, the World Health Organization and CDC reported a growing trend in the increasing number of deaths caused by heart diseases [2, 3].

New methods have been introduced in medicine to a patient-specific. The physicians in fighting the increasing trend of heart disease incidence to protect human life. One of the techniques introduced is patient-specific numerical modelling. Computational Fluid Dynamics (CFD) is the most frequently used simulation method used in the field of blood flow simulations. Nowadays, such methods are used routinely in a variety of applications ranging from modelling vessel prosthetics to the operation of artificial heart valves [4]. CFD is also frequently used to model heart malefactions. Such an approach was used in the case of chronic stenosis of the blood artery [5]. The research objective was to study the ill effects on blood flow. To increase the accuracy of the results, the 3D CT scan was made to reproduce the actual vessel geometry used in the simulation [6, 7].

[1]Department of Thermal Technology, Faculty of Environmental and Energy Engineering, Silesian University of Technology, Gliwice, Poland.
* Corresponding author: bartlomiej.melka@polsl.pl.
[2] Department of Systems Biology and Engineering, Faculty of Automatic Control, Electronics and Computer Science, Silesian University of Technology, Gliwice, Poland.
[3] Department of Diagnostic Imaging, Silesian Center for Heart Diseases, Zabrze, Poland.

The building up of plaque deposition may be one of many reasons for coronary artery disease (CAD), which causes abnormalities in blood flow resulting in a reduced supply of oxygen and other vital nutrients to the heart. Studies show that the left coronary artery (LCA) is more prone to plaque formation compared to the right coronary artery (RCA) [8]. It is caused mainly by uniform flow in RCA compared to LCA. The local wall shear stress in the LCA is low and intensively oscillating, especially in areas of bifurcation [9].

The presented study aims to perform a blood flow through two LCA geometries and analyze the differences in the flow behaviour for a typical LCA case with bifurcation and a rarer case where trifurcation is present. As a result, it will be possible to identify locations prone to plaque deposition, the determination of which may be necessary for proper patient diagnosis and, in the future, for an effective treatment or prevention.

15.2. Mathematical model

Every fluid moving within the model boundaries is subjected to general mass and momentum conservation equations. Such an approach is used to ensure the simulation's proper course.

The mass conservation equation:

$$\frac{\partial \rho}{\partial t} + \nabla(p\vec{v}) = S_M \tag{1}$$

The momentum conservation equations:

$$\frac{\partial}{\partial t}(\rho\vec{v}) + \nabla(\rho\vec{v}) = -\nabla \mathrm{p} + \nabla\bar{\tau} + \rho\vec{g} + \vec{F} \tag{2}$$

where: ρ is a fluid density, t is time, $\vec{v}$ represents velocity vector field, $\bar{\tau}$ is stress tensor, p is static pressure, $\rho\vec{g}$ and $\vec{F}$ are the gravitational body force and external body forces

When performing simulation in ANSYS Fluent package, choosing the most suitable model is essential to obtain the intended effect and reflect the flow behaviour occurring in blood vessels. To carry out the simulation, it is necessary to correctly identify the principles of flow behavior in biofluids. The viscosity value depends on the share rate and shear stress. In this study, the Carreau model has been selected [12].

The Carreau model's viscosity and parameters η, k, and n are fluid dependents. k is the time constant; n is the power-law exponent (described in non-Newton power-law), and η_0 and η_∞ are the upper and lower viscosity limits, corresponding to low and high shear stresses, respectively

The Carreau viscosity (η_c) can be calculated as:

$$\eta_c = \eta_\infty + (\eta_0 - \eta_\infty)[1 + k^2\gamma^2]^{\frac{n-1}{2}} \quad (3)$$

where:

$$\gamma = \sqrt{\frac{1}{2}\Pi}$$

The two coefficients, k, and n are empirically determined [15] and Π denotes the second invariant strain tensor. The values of the coefficients are taken as: η_0 = 0.056 Pa s, η∞ = 0.00345 Pa s, k = 3.313 s and n = 0.3568

The OSI measures the oscillation of shear stresses at the arterial wall and is computed from Eq. (4).

$$OSI = \frac{1}{2}\left[1 - \frac{\left|\int_0^T \tau_w dt\right|}{\int_0^T |\tau_w| dt}\right] \quad (4)$$

where τ is the cardiac period and τ_w is the stress at the artery wall. Wall Shear Stress (WSS) represents the mean shear stresses at the artery wall obtained from Eq. (4).

Wall shear stress was calculated on the base of Eq. (5).

$$\text{WSS} = \frac{1}{T}\left[1 - \int_0^T |\tau_w| dt\right] \quad (5)$$

These indicators are essential since they are believed to give an idea of locations that tend to develop atheroma plaque deposition and, therefore, stenosis growth [17, 18].

The model should accurately perform both near-wall calculations and core fluid motion in the presented research. The shear wall stress (WSS) has a vital role in the flow of blood morphotic elements. Therefore it is unacceptable to omit WSS [10] in the computed simulation so that the standard k−ε model could not be used, due to imperfect near-wall computations. To meet the need for both requirements, the model

of $k-\omega$ was proposed however in the current reseach the laminar flow was assumed. The estimated Re number during the cycle did not exeed 3000.

A time-varying velocity profile was used to represent the actual pulsatile nature of blood flow [11]. This implementation provides more detailed results that could reflect the actual heart behaviour. Figure 1 represents the used velocity temporal profile, which was determined by dividing data published in [12] into five parts. The equations of curves describing changes in velocity were adjusted using the sixth-order polynomial. Moreover, the blood flow rate delivered to LCA was estimated as a 2% value of the patient's stroke volume. The user-defined function (UDF) implemented the velocity profile as the inlet boundary condition. UDF will set the proper polynomial for the given time step in running the simulation. Figure 2 shows that the velocity profile has been adjusted so that one cycle lasts about 0.83 s, and it was consistent with a patient pulse of 72 bpm.

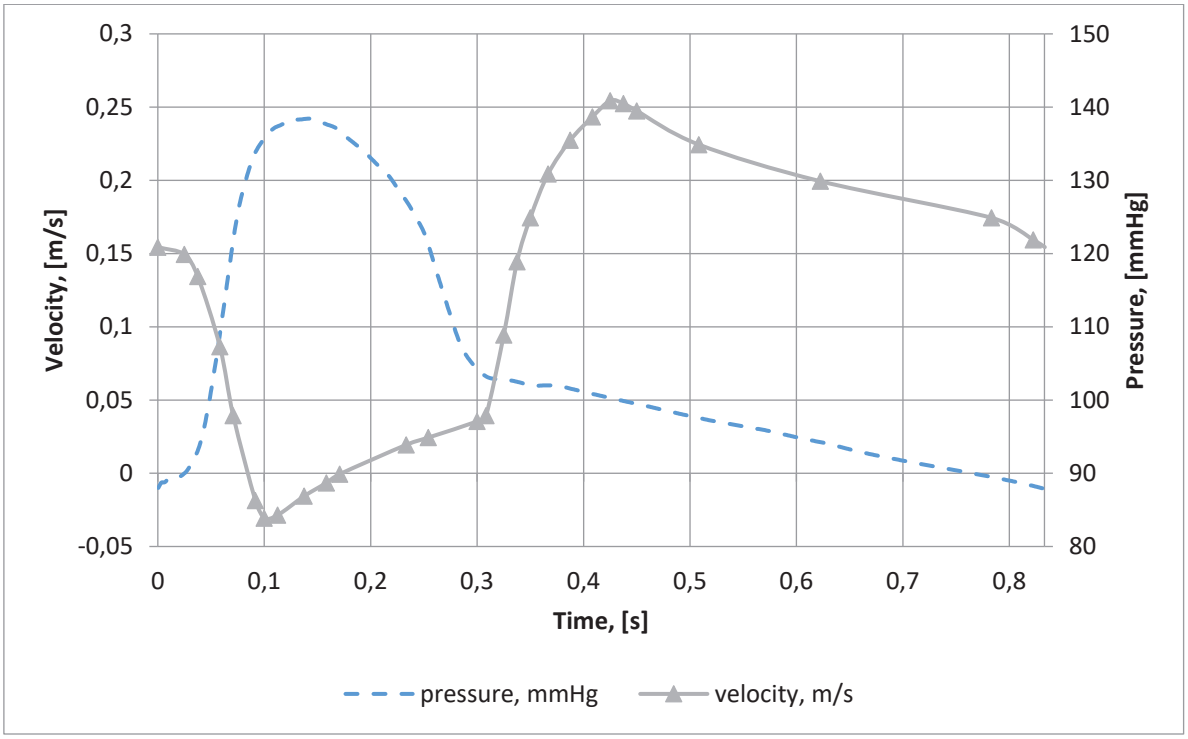

Fig. 1. Inlet velocity and outlet pressures change in a blood vessel
Rys. 1. Zmienny profil prędkości na wlocie oraz zmienny profil ciśnienia na wylocie

A variable velocity profile shown in Fig. 1 was used for the first set of calculations while maintaining constant outlet pressures. The same velocity variable profile at the inlet was used for the second set of calculations. The various pressure was used for the

outlets, which was presented in Fig. 2 using a blue dotted curve. The results obtained from such a procedure allow an estimate of the influence of the pulsatile character of the pressures in the domain on OSI and WSS indicators.

15.2.1. Geometry and discretization procedure

In the simulation, two geometries were examined. The first is a bifurcation geometry shown in Fig. 2 with blunt green. While the second geometry includes trifurcation, and in Fig. 2, it is a geometry with blunt and vibrant green colour. The CT images have been segmented [16]. Produce STL files were later used to define the fluid domain.

Properties. Mesh was created in ANSYS Mesher, using tetrahedral cells. The discretization and the comparison of the parameters of mesh quality for both geometries are shown in Table 1.

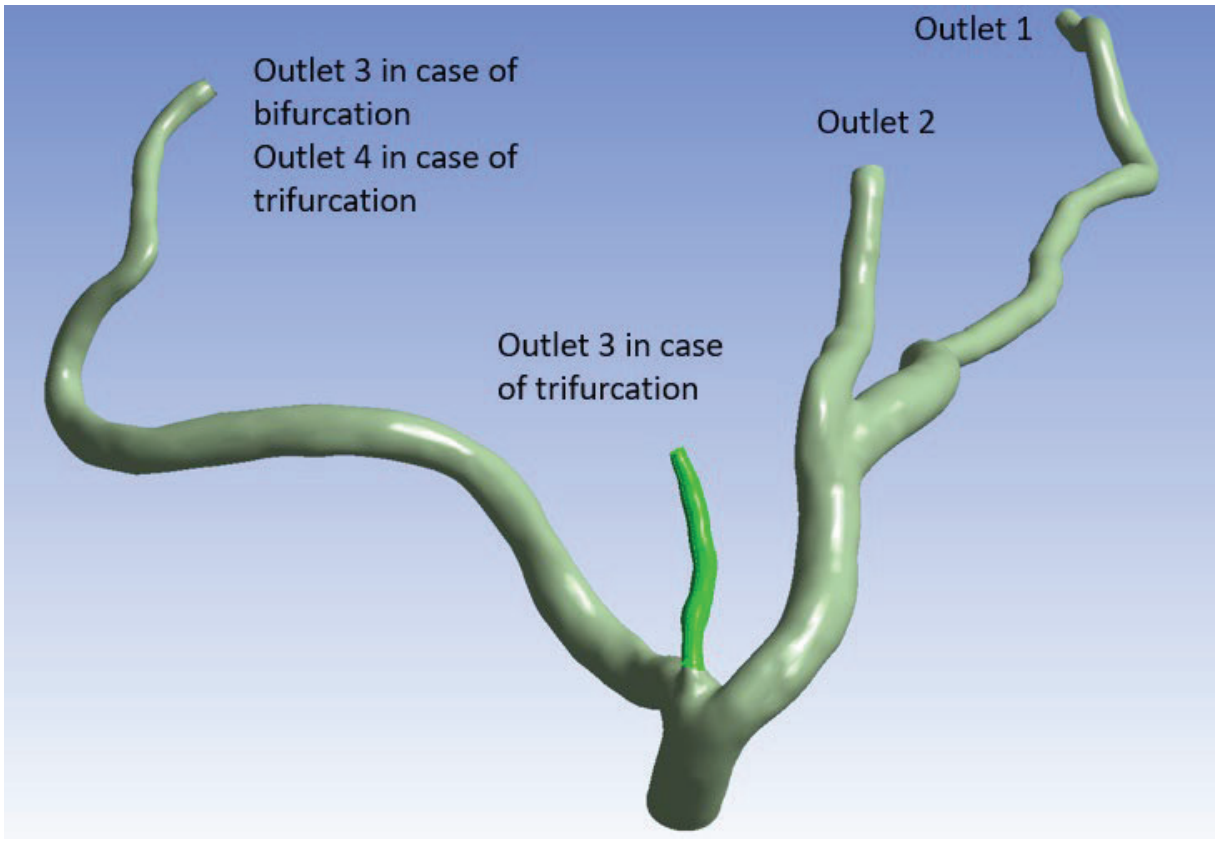

Fig. 2. Geometry comparison in between bifurcation and trifurcation
Rys. 2. Porównanie geometri pomiędzy bifurkacją a trifurkacją

Table 1

Mesh metrics comparison

*	Bifurcation mesh	Trifurcation mesh
Average Element Size	0.25 mm	0.25 mm
Number of Elements	1319788	1338590
Number of Nodes	244986	248878
Average Orthogonal Quality	0.78489	0.78439
Minimal Orthogonal Quality	0.14816	0.31457
Maximal Orthogonal Quality	0.99487	0.99517

15.3. Results and discussion

For both geometries with bifurcation and trifurcation, calculations were performed for two scenarios. The first scenario assumed a constant outlet pressure of 0 Pa, while the second scenario remaining boundary conditions were listed in Section 1.2. As a result of the performed calculations, contours corresponding to WSS and OSI indicators were created.

The resulting OSI and WSS contours show a high probability of atherosclerotic plaque deposition. In the case of OSI, special attention should be paid to locations with a high value of this factor. On the contrary, in the case of WSS, attention should be paid to low values, as the high values will suggest sweeping off the plaque [17, 18].

In Fig. 3 a), a black circle can indicate the site of the plaque diagnosed at the stage of performing geometry scans. This means that the performed calculations indicated the probability of new plaque deposition in the area where calcification was diagnosed

During the calculations, no significant differences were found in the cases for variable and constant outlet pressure. The only difference was the case of bifurcation. Slightly increased OSI values can be observed at 0.32 compared to 0.28 in trifurcation geometries. A similar characteristic can be seen in the WSS values. Lower values at the level of 2.21 Pa occur in the domain with bifurcation and in the domain with trifurcation of values at 2.30 Pa. The flowing blood has more drainage possibilities than trifurcation, so it does not accumulate in the branch with the largest cross-section area.

Fig. 4 and Fig. 5 show the magnitudes of the mass flow rates in case of changing velocity profiles. The flows are distributed accordingly to cross-section areas of a different branch. For example, for the outlet with the largest cross-section area, the blood flow is 7.25 ml/min compared to 1.57 ml/min in the smallest cross-section area. The mass balance remained at the level of 0.01 ml/min, which proves that the blood mass is conserved

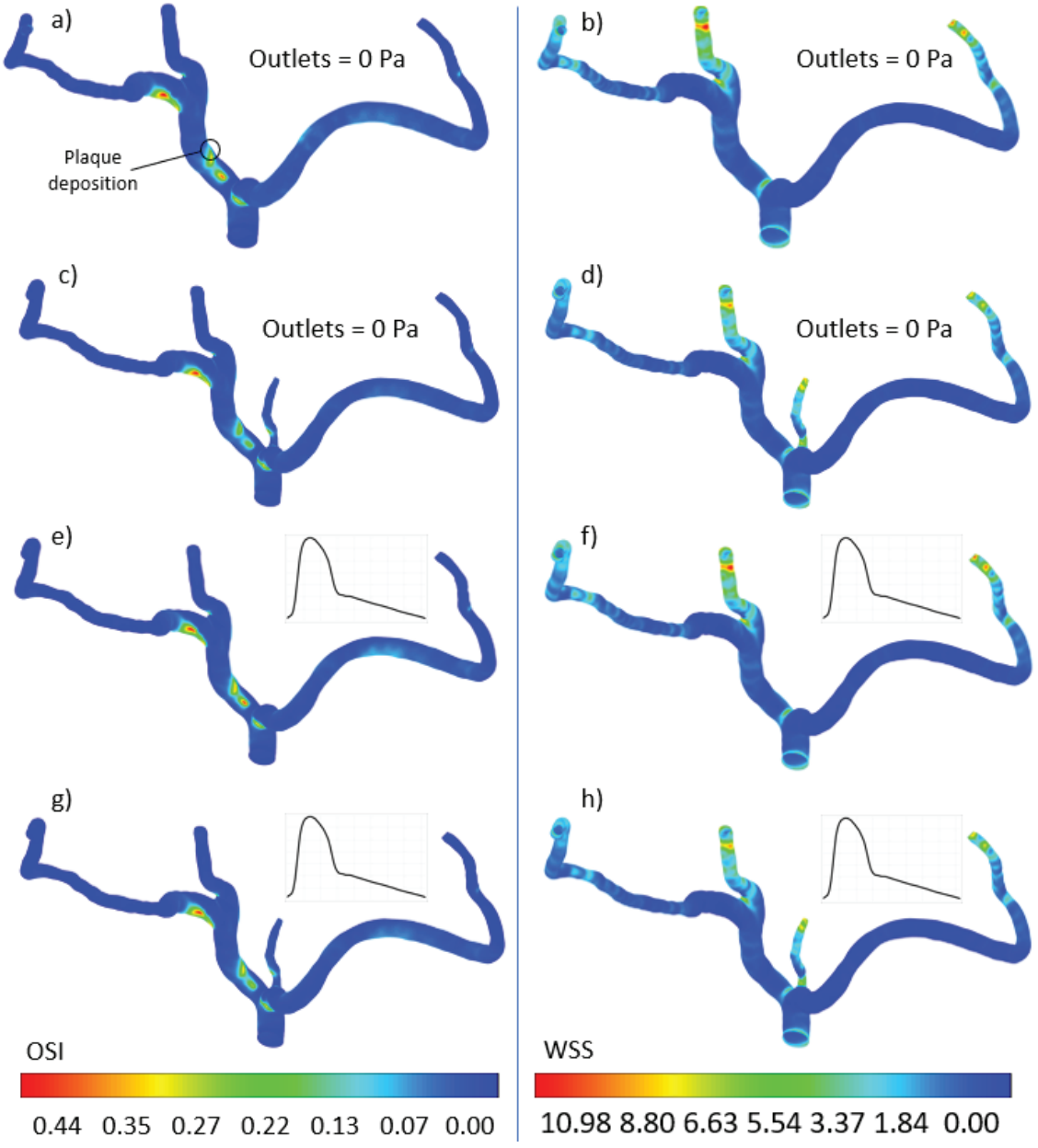

Fig. 3. Wall contours of OSI (left) and WSS (right): a) and b) bifurcation geometry with constant pressure outlets, c) and d) trifurcation geometry with constant pressure outlets, e) and f) bifurcation geometry with pulsatile pressure outlets, g) and h) trifurcation geometry with pulsatile pressure outlets

Rys. 3. Kontury OSI (po lewej) i WSS (po prawej): a) i b) geometria bifurkacji ze stałym profilem ciśnienia wylotowego, c) i d) geometria trifurkacji ze stałym profilem ciśnienia wylotowego, e) i f) geometria rozgałęzienia ze pulsacyjnym profilem ciśnienia na wylocie, g) i h) geometria trifurkacji z pulsacyjnym profilem ciśnienia na wylocie

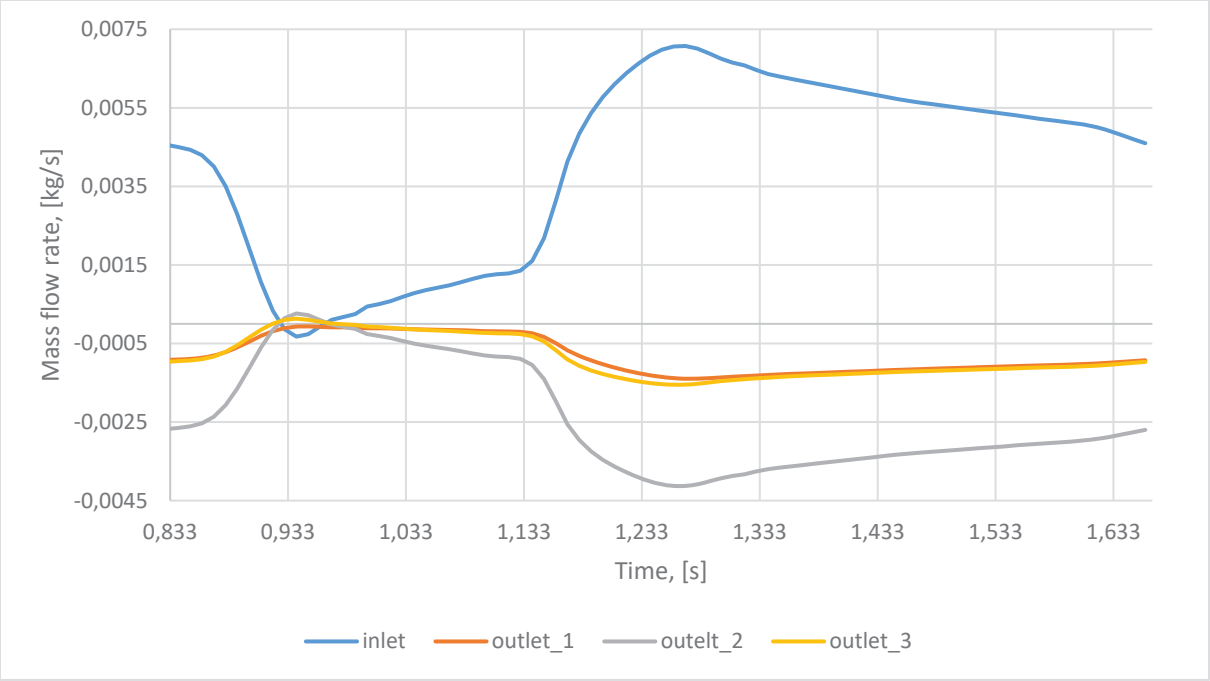

Fig. 4. Mass flow rates in bifurcation with changing velocity profile
Rys. 4. Przepływ masowy przez geometrię bifurkacji ze zmienną prędkością wlotową

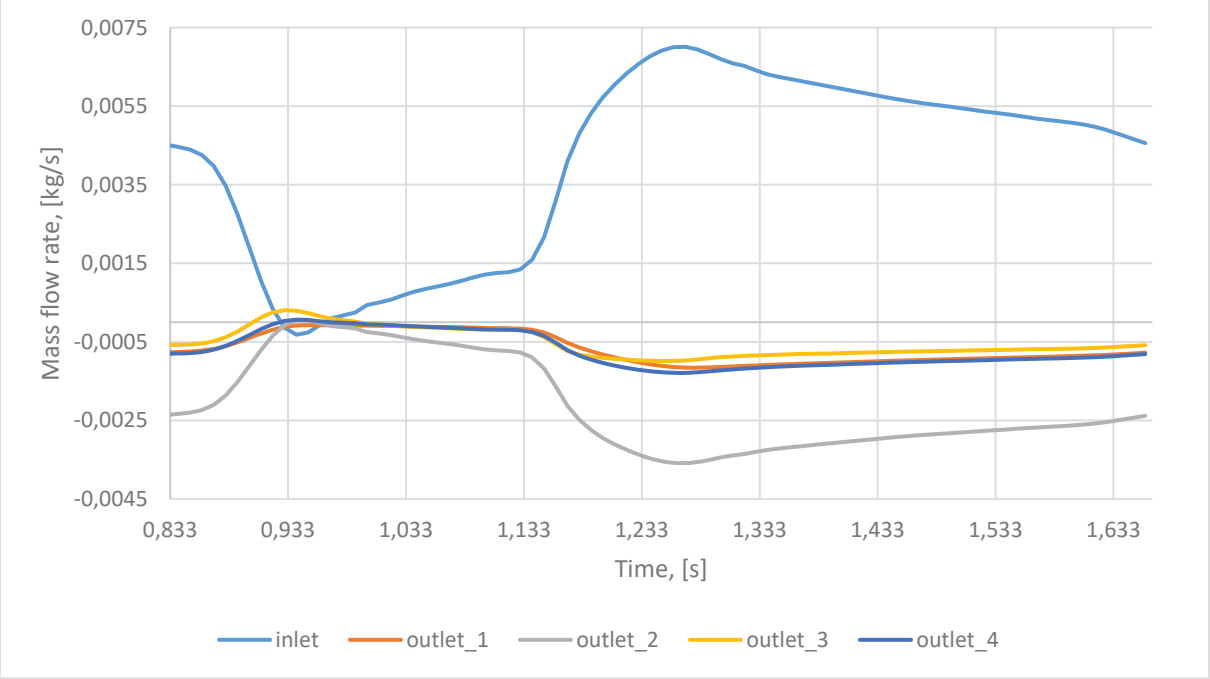

Fig. 5. Mass flow rates in trifurcation with changing velocity profile
Rys. 5. Przepływ masowy przez geometrię trifurkacji ze zmienną prędkością wlotową

15.4. Conclusions

The work was aimed at numerical simulations for two different geometries, which were then used to test the calculations on two different boundary conditions. One of the conditions was to set a variable velocity profile with the simultaneous setting of constant outlet pressures. The second case was the setting of variable inlet and outlet pressures.

The obtained OSI and WSS contours identify areas with a high potential for plaque deposition. The indexes, as mentioned above, indicated, among other things, where the atherosclerotic plaque was deposited in the patient's coronary arteries. The tool could potentially be used to predict the sites of plaque deposition

The obtained results are the basis for the master thesis. It is worth mentioning that the results need to be refined. Particular emphasis should be placed on the quality of the mesh in future calculations and the improvement of the UDF to better reflect the conditions prevailing in the heart.

Acknowledgements

This research is supported by National Science Centre (Poland) project No. 2017/27/B/ST8/01046 and project No. 2019/34/H/ST8/00624. This help is gratefully acknowledged.

Bibliography

1. C.J. McAloon et al.: The changing face of cardiovascular disease 2000–2012: An analysis of the world health organization global health estimates data, *Int. J. Cardiol.*, vol. 224, 2016, pp. 256–264, doi: 10.1016/j.ijcard.2016.09.026.
2. World Health Organization (WHO): The top ten leading causes of death by broad income group, *Fact sheet*, vol. 8, no. 3, 2009, pp. 1–5.
3. “CDC National Health Report Highlights CS251163,” 2012, [Online]. Available: https://www.cdc.gov/healthreport/publications/compendium.pdf.
4. H.A. Simon, L. Ge, F. Sotiropoulos, A.P. Yoganathan: Simulation of the three--dimensional hinge flow fields of a bileaflet mechanical heart valve under aortic conditions, *Ann. Biomed. Eng.*, vol. 38, no. 3, 2010, pp. 841–853, doi: 10.1007/s10439-009-9857-0.

5. T. Kuribara et al.: Preoperatively estimated graft flow rate contributes to the improvement of hemodynamics in revascularization for Moyamoya disease, *J. Stroke Cerebrovasc. Dis.*, vol. 30, no. 1, 2021, p. 105450, doi: 10.1016/j.jstrokecerebrovasdis.2020.105450.
6. W. Wu et al.: 3D reconstruction of coronary artery bifurcations from coronary angiography and optical coherence tomography: feasibility, validation, and reproducibility, *Sci. Rep.*, vol. 10, no. 1, 2020, pp. 1–11, doi: 10.1038/s41598--020-74264-w.
7. D. Lopes, H. Puga, J. Teixeira, R. Lima: Blood flow simulations in patient-specific geometries of the carotid artery: A systematic review, *J. Biomech.*, vol. 111, 2020, p. 110019, doi: 10.1016/j.jbiomech.2020.110019.
8. B.T. Chan, E. Lim, K.H. Chee, N.A. Abu Osman: Review on CFD simulation in heart with dilated cardiomyopathy and myocardial infarction, *Comput. Biol. Med.*, vol. 43, no. 4, 2013, pp. 377–385, doi: 10.1016/j.compbiomed.2013.01.013.
9. J.V. Soulis, T.M. Farmakis, G.D. Giannoglou, G.E. Louridas: Wall shear stress in normal left coronary artery tree, *J. Biomech.*, vol. 39, no. 4, 2006, pp. 742–749, doi: 10.1016/j.jbiomech.2004.12.026.
10. B. Su, J.M. Zhang, H. Zou, D. Ghista, T.T. Le, C. Chin: Generating wall shear stress for coronary artery in real-time using neural networks: Feasibility and initial results based on idealized models, *Comput. Biol. Med.*, vol. 126, no. September, 2020, p. 104038, doi: 10.1016/j.compbiomed.2020.104038.
11. M. Lodi Rizzini et al.: Does the inflow velocity profile influence physiologically relevant flow patterns in computational hemodynamic models of left anterior descending coronary artery?, *Med. Eng. Phys.*, vol. 82, pp. 58–69, 2020, doi: 10.1016/j.medengphy.2020.07.001.
12. M. Abbasian, M. Shams, Z. Valizadeh, A. Moshfegh, A. Javadzadegan, S. Cheng, Effects of different non-Newtonian models on unsteady blood flow hemodynamics in patient-specific arterial models with in-vivo validation, *Comput. Methods Programs Biomed.*, vol. 186, 2020, p. 105185, doi: 10.1016/j.cmpb.2019.105185.
13. J. Wasilewski, K. Mirota, S. Peryt-Stawiarska, A. Nowakowski, L. Poloński, M. Zembala: Wprowadzenie do numerycznej mechaniki płynu na podstawie komputerowej symulacji przepływu w lewej tętnicy wieńcowej, *Kardiochirurgia i Torakochirurgia Pol.*, vol. 9, no. 3, 2012, pp. 366–374, doi: 10.5114/kitp.2012.30851.

14. M. Abbasian, M. Shams, Z. Valizadeh, A. Moshfegh, A. Javadzadegan, S. Cheng: Effects of different non-Newtonian models on unsteady blood flow hemodynamics in patient-specific arterial models with in-vivo validation, *Comput. Methods Programs Biomed.*, vol. 186, 2020, p. 105185, doi: 10.1016/j.cmpb.2019.105185.
15. S. Tabakova, E. Nikolova, S. Radev: Carreau model for oscillatory blood flow in a tube, *AIP Conf. Proc.*, vol. 1629, no. February, 2014, pp. 336–343, doi: 10.1063/1.4902290.
16. B. Berthier, R. Bouzerar, C. Legallais: Blood flow patterns in an anatomically realistic coronary vessel: Influence of three different reconstruction methods, *J. Biomech.*, vol. 35, no. 10, 2002, pp. 1347–1356, doi: 10.1016/S0021-9290(02)00179-3.
17. A.S. Anayiotos, S.A. Jones, D.P. Giddens, S. Glagov, C.K. Zarins: Shear stress at a compliant model of the human carotid bifurcation, *J. Biomech. Eng.*, vol. 116, no. 1, pp. 98–106, 1994, doi: 10.1115/1.2895710.
18. D.N. Ku, D.P. Giddens, C.K. Zarins, S. Glagov: Pulsatile flow and atherosclerosis in the human carotid bifurcation. Positive correlation between plaque location and low and oscillating shear stress, *Arteriosclerosis*, vol. 5, no. 3, 1985, pp. 293–302, doi: 10.1161/01.atv.5.3.293.

NUMERICAL MODELING OF BLOOD FLOW IN BIFURCATION AND TRIFURCATION GEOMETRIES W USE OF DIFFERENT BOUNDARY CONDITIONS

Abstract

The presented work compares the flow through the coronary vessels under different boundary conditions. The geometries were developed as a result of patient scans. It is a modern and non-invasive diagnostic method to achieve highly accurate results. The simulations' results will allow us to identify places susceptible to plaque deposition, which causes collapses or death.

The obtained results for the cases with constant and variable pressure turned out to be similar. The only difference was the case of bifurcation. Slightly increased OSI values result from a lower number of outflows from the domain. The flowing blood has more

drainage possibilities than trifurcation, so it does not accumulate in the ebb with the largest cross-section area. Other than the conclusion, there were no significant discrepancies indicative of inaccuracies in any of the methods.

For future simulations, the generated mesh should be refined, and the model's sensitivity should be assessed. The next step is to improve the UDF to give the most accurate results compared to those measured.

Keywords: bifurcation, trifurcation, blood, coronary vessel, CFD